Department of the Navy
Naval Ordnance Test Station
Contract N123(60530)24917A

ON THE MECHANISM OF CAVITATION DAMAGE BY NON-HEMISPHERICAL CAVITIES COLLAPSING IN CONTACT WITH A SOLID BOUNDARY

by

Charl F. Naudé and Albert T. Ellis

Hydrodynamics Laboratory
CALIFORNIA INSTITUTE OF TECHNOLOGY
Pasadena, California

Report No. E-108.7 July 1960

Department of the Navy
Naval Ordnance Test Station
Contract N123(60530)24917A

ON THE MECHANISM OF CAVITATION DAMAGE BY NON-HEMISPHERICAL CAVITIES COLLAPSING IN CONTACT WITH A SOLID BOUNDARY

by

Charl F. Naudé and Albert T. Ellis

Hydrodynamics Laboratory
California Institute of Technology
Pasadena, California

Report No. E-108.7

July 1960

ACKNOWLEDGEMENTS

The authors wish to express their sincere appreciation for the competent assistance of Prof. P. A. Lagerstrom with the theoretical work.

Financial support from the following sources made this study possible.

1. Research Bursary from the South Africa Council for Scientific and Industrial Research (1956-1959)
2. Queen Victoria Stipendium from the University of Stellenbosch, South Africa (1957-1959)
3. Francis J. Cole fellowship from the California Institute of Technology

The experimental work was carried on with support from

1. National Science Foundation Grant G-2586.
2. U.S. Navy Bureau of Ordnance contract NOrd 16200.
3. Office of Naval Research equipment loan NOnr 218100.
4. U.S. Naval Ordnance Test Station Contract N123(60530)21703A.
5. U.S. Naval Ordnance Test Station Contract N123(60530)24917A.

ABSTRACT

A perfect fluid theory, which neglects the effect of gravity, and which assumes that the pressure inside a cavitation bubble remains constant during the collapse process, is given for the case of a non-hemispherical, but axially symmetric cavity which collapses in contact with a solid boundary. The theory suggests the possibility that such a cavity may deform to the extent that its wall strikes the solid boundary before minimum cavity volume is reached. High speed motion pictures of cavities generated by spark methods are used to test the theory experimentally. Agreement between theory and experiment is good for the range of experimental cavities considered, and the phenomenon of the cavity wall striking the solid boundary does indeed occur. Studies of damage by cavities of this type on soft aluminum samples reveals that pressures caused by the cavity wall striking the boundary are higher than those resulting from a compression of gases inside the cavity, and are responsible for the damage.

INTRODUCTION

Until the present most of the theoretical efforts to explain damage by cavitation were spent in attempts to understand the collapse process of spherical cavities in an infinite liquid. This problem is complicated because effects of compressibility, surface tension and viscosity play an important role. Furthermore, the behavior of the gaseous substances inside the cavity, and especially the non-equilibrium behavior of the included vapor under high rates of compression are not known.

It has been realized for some time that the spherical shape of a collapsing cavity is unstable in the sense that a finite initial perturbation of the spherical shape will grow very large as the cavity

collapses. This instability is demonstrated elegantly in a publication by Plesset and Mitchell [1].

In view of the asymmetric perturbing influences which act on a cavity collapsing close to, or in contact with, a solid boundary, it appears reasonable to expect that cavities which do not remain spherically symmetric during collapse could play an important role in cavitation damage. Eisenberg [2] recognized the possibility in 1950 when he speculated that jets formed during the unsymmetrical collapse of cavitation bubbles could be responsible for the damage. Kornfeld and Suvorov [3] also suggested this mechanism of damage in a 1944 publication.

The object of the present study is to investigate the collapse process of, and the mechanism of damage by, cavities in contact with a solid boundary which collapse non-hemispherically mainly as a result of initial perturbations of the hemispherical shape. It is hoped that such a study may be the first step in understanding the mechanism of damage by cavities which collapse non-hemispherically as a result of other effects.

THEORY

Consider a cavity which is symmetric about a line normal to a solid plane boundary. A spherical coordinate system as shown in figure 1 is chosen for the formulation of the problem.

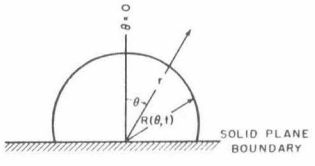

Figure 1. The Spherical Coordinate System

The following assumptions will be used:

1) The liquid is incompressible.

2) The pressure inside the cavity is constant.

3) The effect of viscosity is negligible.

4) Surface tension and adhesion are negligible.

5) The effect of gravity is negligible.

A brief discussion of the validity of the assumptions follows at the end of the theoretical work.

With the assumptions listed above the problem is reduced to solving the differential equation

$$\nabla^2 \Phi(r, \theta, t) = 0 \tag{1}$$

where Φ is a scalar potential function such that $\nabla \Phi = \underset{\sim}{q}$, the velocity vector. The following boundary conditions must be satisfied:

$$\Phi \longrightarrow 0 \quad \text{as} \quad r \longrightarrow \infty \tag{2}$$

$$\frac{1}{r} \frac{\partial \Phi}{\partial \theta} = 0 \quad \text{on} \quad \theta = \frac{\pi}{2} \tag{3}$$

$$\left[\frac{\partial \Phi}{\partial t} + \frac{1}{2} \left(\frac{\partial \Phi}{\partial r} \right)^2 + \frac{1}{2r^2} \left(\frac{\partial \Phi}{\partial \theta} \right)^2 \right]_{r=R} = \frac{p_\infty - p_c}{\rho} \tag{4}$$

where p_∞ and p_c are the constant pressures at infinity and in the cavity respectively, and ρ is the liquid density.

$$\left[\frac{\partial \Phi}{\partial r} - \frac{1}{r^2} \frac{\partial \Phi}{\partial \theta} \cdot \frac{\partial R}{\partial \theta} \right]_{r=R} = \frac{\partial R}{\partial t} \tag{5}$$

where t is the time. A solution to Equation (1) which satisfies Equations (2) and (3) is

$$\Phi (r, \theta, t) = \frac{\phi_o(t)}{r} + \sum_{n=1}^{\infty} \phi_{2n}(t) \frac{1}{r^{2n+1}} P_{2n}(\cos \theta) \tag{6}$$

where $P_{2n}(\cos \theta)$ are Legendre polynomials, and ϕ_o and ϕ_{2n} are

time dependent coefficients in the expansion. One is thus led to express

$$R(\theta, t) = R_o(t) + \sum_{n=1}^{\infty} R_{2n}(t) P_{2n}(\cos\theta) \tag{7}$$

where R_o and R_{2n} are time dependent coefficients in the expansion. The procedure for solution is then to substitute Equations (6) and (7) into Equations (4) and (5), thus obtaining the differential equations that must be satisfied by ϕ_o, ϕ_{2n}, R_o and R_{2n}. These differential equations are then solved with the initial conditions.

$$R(\theta, 0) = R_o(0) + \sum_{n=1}^{\infty} R_{2n}(0) P_{2n}(\cos\theta) \tag{8}$$

$$\frac{dR}{dt}(\theta, 0) = \sum_{n=1}^{\infty} \frac{dR_{2n}}{dt}(0) P_{2n}(\cos\theta). \tag{9}$$

The quantities $R_o(0)$, $R_{2n}(0)$ and $\frac{dR_{2n}}{dt}(0)$ are specified. Time $t = 0$ is chosen such that $\frac{dR_o}{dt} = 0$.

In view of the nonlinearity of Equations (4) and (5) an attempt is made to obtain a perturbation solution for restricted values of the quantities ϕ_{2n} and R_{2n}.

First Perturbation Procedure

Assume that the sums on the right hand sides of Equations (6) and (7) are small compared to ϕ_o/r and R_o respectively, so that all interactions between terms in these sums may be neglected. Substituting Equations (6) and (7) into Equations (4) and (5), and using the orthogonality of Legendre Polynomials one finds

$$\phi_o = \left[\frac{2}{3} \frac{p_\infty - p_c}{\rho} R_o(R_o^3(0) - R_o^3)\right]^{1/2} \tag{10}$$

$$t = \frac{R_o(0)}{\left[\frac{2}{3}\frac{p_\infty - p_c}{\rho}\right]^{1/2}} \int_{\frac{R_o}{R_o(0)}}^{1} \frac{d\xi}{\left[\frac{1}{\xi^3} - 1\right]^{1/2}} \tag{11}$$

The time at which R_o becomes zero is given by

$$T = \frac{.915\, R_o(0)}{\left[\frac{p_\infty - p_c}{\rho}\right]^{1/2}} . \tag{12}$$

The $P_o(\cos\theta)$ component of the bubble thus still satisfies the Rayleigh theory.

With the substitutions $\left[\frac{R_o(0)}{R_o}\right]^3 = x$ and $\frac{R_{2n}}{R_{2n}(0)} = y_{2n}$ the following equation is obtained for the R_{2n}:

$$(1-x)\,x\,\frac{d^2 y_{2n}}{dx^2} + \left(\frac{1}{3} - \frac{5}{6}x\right)\frac{dy_{2n}}{dx} - \frac{1}{6}(2n-1)y_{2n} = 0. \tag{13}$$

Equation (13) is of hypergeometric form [4], with

$$\begin{aligned} c &= \frac{1}{3} \\ a(n) &= \frac{1}{12}\left(-1 + i(48n-25)^{1/2}\right) \\ b(n) &= \frac{1}{12}\left(-1 - i(48n-25)^{1/2}\right) \end{aligned} \tag{14}$$

and the general solution can be written in the form [4]

$$\begin{aligned} y_{2n} &= A_{2n}\, x^{-a} F\left(a, a+\tfrac{2}{3}; \tfrac{1}{2}; 1-\tfrac{1}{x}\right) + B_{2n}\, x^{-a}(1-x)^{1/2} F\left(-b+\tfrac{1}{3}; -b+1; \tfrac{3}{2}; 1-\tfrac{1}{x}\right) \\ &= A_{2n}\, y_{2n_1} + B_{2n}\, y_{2n_2} \end{aligned} \tag{15}$$

where the hypergeometric function F is given by

$$F(\alpha, \beta; \gamma; z) = \sum_{m=o}^{\infty} \frac{(\alpha)_m (\beta)_m}{(\gamma)_m} z^m \tag{16}$$

and

$$(\alpha)_m = \Gamma(\alpha + m)/\Gamma(\alpha).$$

The constants A_{2n} and B_{2n} are readily determined from the initial conditions

$$\begin{aligned} A_{2n} &= 1 \\ B_{2n} &= .892\, \frac{dy_{2n}}{d(t/T)} . \end{aligned} \tag{17}$$

The solutions y_{2n_1} and y_{2n_2} are shown in figures 2 and 3 respectively as functions of $R_o/R_o(0)$. The solutions given here are the same as the one obtained by Plesset and Mitchell [1]. In the present case odd Legendre Polynomials have been eliminated because of the boundary.

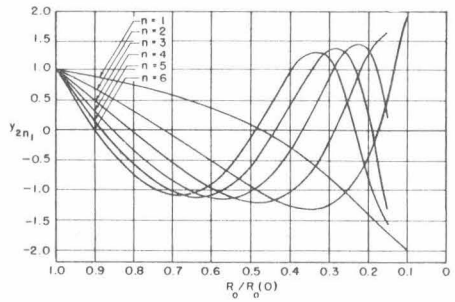

Figure 2. The first solution to Equation (13), y_{2n_1}, as a function of $R_o/R_o(0)$

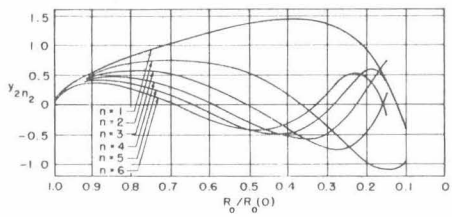

Figure 3. The second solution to Equation (13), y_{2n_2}, as a function of $R_o/R_o(0)$

Both y_{2n_1} and y_{2n_2} exhibit an interesting characteristic, namely that they oscillate with increasing amplitude and frequency as R_o approaches zero. Physically this implies that a finite initial perturbation, $\sum_{n=1}^{\infty} R_{2n}P_{2n}$, of the hemispherical shape could grow so large that the cavity wall could strike the solid boundary before R_o becomes zero. Because of the large perturbation quantities that are involved at this stage of collapse it is not possible to apply the simple theory that has been presented. As far as damage by cavitation is concerned the suggestions offered by this theory are interesting enough to stimulate further investigation.

Second Perturbation Procedure

Consider a somewhat more physically realistic cavity for which $R_o > R_2 > R_4 > R_6$, and R_{2n} is negligibly small for $n \geq 4$ in Equation (7). The most significant interactions between terms in the sums of Equations (6) and (7) will be retained in this analysis in an attempt to obtain a better description of the behavior of the cavity when perturbations of the hemispherical shape become fairly large.

One then finds that R_o and ϕ still satisfy Equations (10) and (11) within terms of order $\left[\frac{R_2(0)}{R_o(0)}\right]^2$.

$\frac{R_{2n}}{R_{2n}(0)} = y'_{2n}$ now satisfies

$$(1-x)x\frac{d^2y'_{2n}}{dx^2} + (\frac{1}{3} - \frac{5}{6}x)\frac{dy'_{2n}}{dx} - \frac{1}{6}(2n-1)y'_{2n} = F_{2n}(x) \qquad (18)$$

for $n = 1$, 2 and 3.

$$F_2 = 0 + O(\frac{R_2(0)}{R_o(0)}) \qquad (19)$$

$$F_4 = -\frac{1}{315}\left[\frac{R_2^2(0)}{R_o(0)R_4(0)}\right](x^{-2/3})\left[(49x+32)y_2'^2 + 474(x-1)x\frac{dy'_2}{dx}y'_2 - 639(x-1)x^2(\frac{dy'_2}{dx})^2\right] + O(\frac{R_2(0)}{R_o(0)}) \qquad (20)$$

$$F_6 = -\frac{1}{297}\left[\frac{R_o(0)R_4(0)}{R_o(0)R_6(0)}\right](x^{-2/3})\left[(129x+96)y'_2y'_4 + 765(x-1)x\frac{dy'_2}{dx}y'_4 + 639(x-1)xy'_2\frac{dy'_4}{dx} - 1485(x-1)x^2\frac{dy'_2}{dx}\frac{dy'_4}{dx}\right] + \frac{1}{3465}\left[\frac{R_2^3(0)}{R_o^2(0)R_6(0)}\right](x^{-1/3})$$

$$\left[(3418x-4228)y_2'^3 - 17328(x-1)xy_2'^2\frac{dy'_2}{dx} + 19395(x-1)x^2y'_2(\frac{dy'_2}{dx})^2\right] + O(\frac{R_2(0)}{R_o(0)}). \qquad (21)$$

The only difference between Equations (13) and (18) is that (18) contains a forcing function F_{2n}. One may thus write

$$y'_{2n} = y_{2n} + y_{2np} \tag{22}$$

where y_{2np} is a particular integral of Equation (18). The particular integral can be found readily by variation of parameters [5]

$$y_{2np} = -u_{2n}\int_1^x \left[\frac{1}{u_{2n}^2(x-1)^{1/2}x^{1/3}} \int_1^x \frac{u_{2n}F_{2n}}{(x-1)^{1/2}x^{2/3}}\,dx\right] dx \tag{23}$$

where u_{2n} is a solution to the homogeneous Equation (13). The lower limits of the integrals have been chosen in such a way that y_{2np} and $\frac{dy_{2np}}{dt}$ vanish initially, so that Equations (17) are still valid. The singularities of the integrals at $x=1$ are integrable, and the singularities at the zeros of u_{2n} can be shown to be removable.

Because $F_2 = 0$, y'_2 can be written in the form

$$y'_2 = y_{2_1} + B_2 y_{2_2}. \tag{24}$$

The function F_4 can then be expressed

$$F_4 = \left[\frac{R_2^2(0)}{R_o(0)R_4(0)}\right]\left[F_{4_1} + B_2 F_{4_2} + B_2^2 F_{4_3}\right] \tag{25}$$

so that

$$y_{4_p} = \left[\frac{R_2(0)}{R_o(0)R_4(0)}\right]\left[y_{4p_1} + B_2 y_{4p_2} + B_2^2 y_{4p_3}\right] \tag{26}$$

where

$$y_{4p_i} = -u_4\int_1^x\left[\frac{1}{u_4^2(x-1)^{1/2}x^{1/3}} \int_1^x \frac{u_4 F_{4_i}}{(x-1)^{1/2}x^{2/3}}\,dx\right] dx. \tag{27}$$

In figure 4 y_{4p_i}, with $i = 1, 2$, and 3, are shown as functions of $R_o/R_o(0)$. Figure 5 is a magnification of the portions of these functions for which $R_o/R_o(0) > 0.4$.

In figure 6 theoretical cavity shapes at different values of $R_o/R_o(0)$ are demonstrated. The initial conditions for this cavity are the same as for the experimental cavity demonstrated in figure 18, and can be specified by $R_o(0) = .225"$, $R_2(0) = .065"$, $R_4(0) = -.0127"$, $B_2 = -.83$,

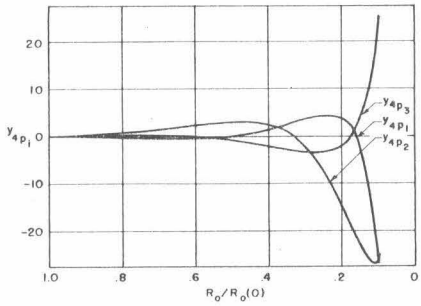

Figure 4. The three components of the particular integral of Equation (18) with n = 2

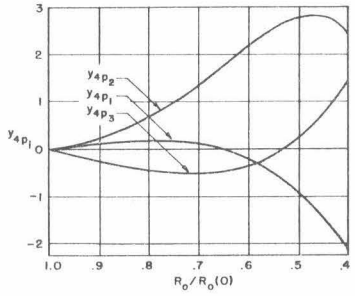

Figure 5. The three components of the particular integral of Equation (18) with n = 2 for $R_o/R_o(0) > 0.4$

$B_4 = -5.45$, $T = 524\mu s$. The jet which enters the cavity and strikes

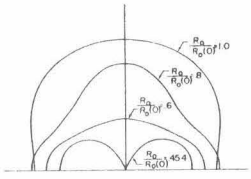

Figure 6. Theoretical cavity shapes for different values of $R_o/R_o(0)$

the solid boundary is evident. The fact that the radius of curvature of the jet becomes zero at the time of impact is not physically realistic, and is probably the result of a breakdown of the perturbation procedure plus the fact that surface tension has been omitted from the theory.

The validity of the assumptions

1) An estimate of the error introduced by neglecting compressibility can be obtained from the work of Gilmore [6]. For a cavity collapsing

in water under a constant pressure difference of 1 atmosphere, the error in cavity radius reaches about 10% when $R_o/R_o(0) = 0.1$.

2) For a vaporous cavity the assumption of constant cavity pressure will become poor when the cavity wall velocity becomes comparable to the velocity of the vapor molecules at the temperature inside the cavity. Assuming isothermal collapse, which is probably pessimistic, the assumption will become poor for a cavity in water when the wall velocity reaches 2000 ft/sec. With a pressure difference of 1 atm. this corresponds to $R_o/R_o(0) = .05$.

3) A rough estimate of the effect of viscosity can be obtained by using the two dimensional boundary layer theory for a suddenly accelerated plane wall. The boundary layer thickness, δ, is given by [7] $\delta \approx 4\sqrt{\nu t}$ where ν is the viscosity and t is the time after the motion began. Replacing t with T from Equation (12) one finds that for cavities with $R_o(0) > .1''$ in water, the boundary layer thickness will reach at most 20% of R_o when $R_o/R_o(0)$ becomes .15, provided the pressure difference is 1 atm. This effect becomes much smaller as $R_o(0)$ is increased.

4) A comparison of surface tension forces with inertia forces shows that for bubbles collapsing in water, under 1 atm. pressure difference, radii of curvature of the order of 10^{-9} ft. have to occur at $R_o/R_o(0) = .05$ before these forces become comparable.

5) A rough calculation based on the work of Cole [8] shows that the effect of the solid boundary greatly supersedes the effect of gravity for cavities of the type considered here.

EXPERIMENTAL RESULTS

Because the convergence of the perturbation theory which was presented could not be proved, and because perturbation quantities become very large during the final stages of collapse, it seemed necessary to perform some experiments to cast more light on the subject.

A series of motion pictures of cavities generated by spark methods were taken with the Ellis Kerr-cell camera [9]. The magnitude of the perturbation of the hemispherical shape was varied by simply changing the distance of the spark gap from the solid boundary. Since indented portions of the cavity wall could not be photographed, an indirect means of observing the jet entering the cavity had to be found. Use of a photoelastic solid boundary proved to be the most successful method.

In figure 7 a typical motion picture record of a cavity collapsing on a CR-39 photoelastic boundary is presented. Frames below one another in vertical columns are consecutive, and columns follow one another from left to right. R_o, R_2, R_4 and R_6 as functions of time were found from a Legendre analysis of the motion pictures. R_o reached its maximum of .244" in frame 9 of the first column. At this time $R_2(0)$ and $R_4(0)$ were .113" and -.0334" respectively. B_2 and B_4 had the values -.57 and -2.4. The time for complete collapse, T, was approximately 570 μs. The small disturbance which originates near the center of the cavity base in frame 12 of column 5 is believed to be the result of the impinging jet.

The large disturbance in frame 9 of column 6 probably corresponds to the compression of gases in the cavity, because afterwards the cavity volume increases again.

In figures 8, 9 and 10 experimental points of $R_o/R_o(0)$ as a function of time, and $R_2/R_2(0)$ and $R_4/R_4(0)$ as functions of $R_o/R_o(0)$

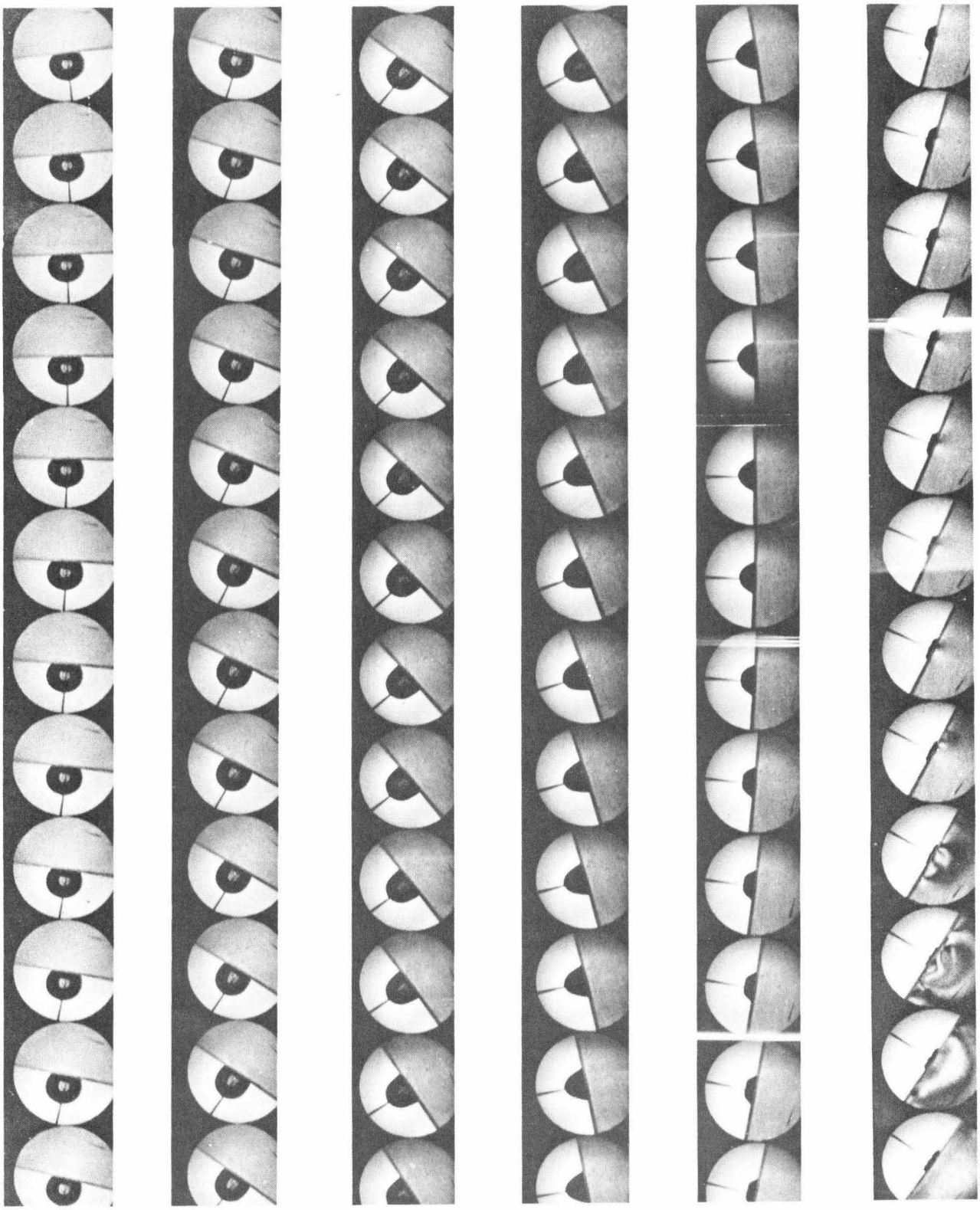

Fig. 7. A cavity collapsing on the CR-39 photoelastic boundary. Time between frames is 10 microseconds.

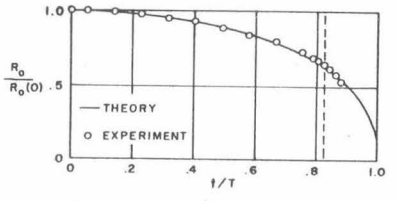

Figure 8. $R_o/R_o(0)$ as a function of t/T for the cavity in figure 7.

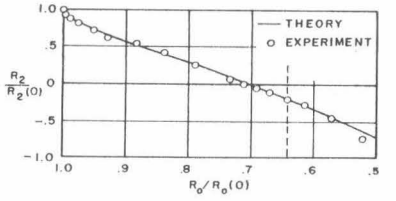

Figure 9. $R_2/R_2(0)$ as a function of $R_o/R_o(0)$ for the cavity in figure 7.

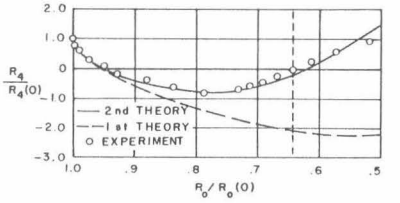

Figure 10. $R_4/R_4(0)$ as a function of $R_o/R_o(0)$ for the cavity in figure 7.

are compared with the theory. Dotted vertical lines in these figures indicate when the cavity became indented. Points to the right of the dotted lines depend on an estimate of the shape of the indented portion which was greatly aided by a knowledge of when the jet struck the solid boundary. The dotted curve in figure 10 shows the results of the first perturbation procedure, while the solid curve was calculated by means of the second perturbation method. Agreement between theory and experiment for this particular cavity was better than average. Considering the scatter of the experimental data, agreement was good in the range of cavities which were considered.

In figures 11 and 12 an attempt was made to obtain a simultaneous

comparison of $R_2/R_2(0)$ for ten different cavities with the theory. Such

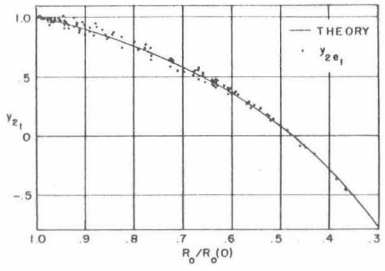

Figure 11. A comparison of experimental points for y_{2e_1} with the theoretical y_{2_1} curve.

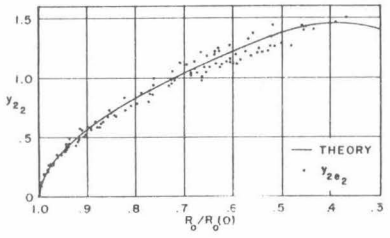

Figure 12. A comparison of experimental points for y_{2e_2} with the theoretical y_{2_2} curve.

a comparison is necessarily based on an apportioning of the difference between theory and experiment to the y_{2_1} and y_{2_2} parts of $R_2/R_2(0)$. The method of apportioning that was used is as follows:

Suppose that at $R_o/R_o(0) = \omega$, an experimental value of $R_2/R_2(0)$ was found to be y_{2e}. The difference ϵ between theory and experiment at this point is then

$$\epsilon = y_2(\omega) - y_{2e}(\omega) = y_{2_1}(\omega) + B_2 y_{2_2}(\omega) - y_{2e}(\omega).$$

One may then write

$$y_{2e}(\omega) = \left[y_{2_1}(\omega) - \epsilon \frac{\left| y_{2_1}(\omega) \right|}{\left| y_{2_1}(\omega) \right| + \left| B_2 y_{2_2}(\omega) \right|} \right] + B_2 \left[y_{2_2}(\omega) - \epsilon \frac{|B_2|}{B_2} \frac{\left| y_{2_2}(\omega) \right|}{\left| y_{2_1}(\omega) \right| + \left| B_2 y_{2_2}(\omega) \right|} \right]$$

$$= y_{2e_1}(\omega) + B_2 y_{2e_2}(\omega).$$

The "experimental" points of y_{2e_1} and y_{2e_2} are then compared with

the theory.

Despite the evident weakness of the method of apportioning, figures 11 and 12 give a good indication of the scatter involved in the experimental results. The experimental points seem to be well grouped around the theoretical curves.

A similar representation of experimental results for $R_4/R_4(0)$ was not attempted, because y_4 is a linear combination of five different functions of $R_o/R_o(0)$.

Experimental data for $R_6/R_6(0)$ was very erratic because the magnitude of y_6 was of the same order as errors in the measurements. These results are not presented.

Although the photoelastic fringes (isochromatics) were of great value in determining the time at which a jet struck the solid boundary, it was not possible to derive quantitative information regarding the pressures which occurred from the fringe patterns because the area over which the pressure acted and the pressure distribution were unknown. Some quantitative information regarding the magnitude of the compression pulse could be obtained with the use of a quartz crystal pressure pickup.

The pickup is shown schematically in figure 13. The crystal Q is glued into the end of an aluminum bar which is made up of tubes C_1, C_2, C_3 and the rod C_4. All these elements are electrically insulated from one another, and thus form connections to four different areas on the back of the crystal. The insulation of C_1, C_2, C_3 and C_4 was achieved by anodizing them before they were glued together. The aluminum plate P forms the connection to the front of the crystal. Troubles from reflections were minimized by lead bar L which was glued to the other end of the unit. Electrical connections to C_2, C_3 and C_4 are obtained with wires

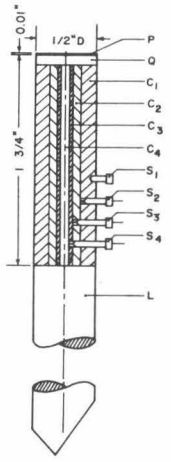

Figure 13. The quartz crystal pickup.

through size 80 holes drilled down the center of 0-80 nylon screws S_2, S_3 and S_4. An 0-80 bress screw S_1 forms the connection to C_1.

In figure 14 the output obtained from C_2 (upper trace) and C_4 (lower trace) with C_1 and C_3 grounded is shown when a 1/16" ball bearing

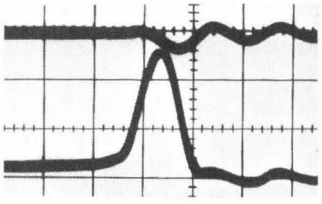

Figure 14. The response of the quartz crystal unit to a 1/16" ball bearing dropped on the center of the crystal.

is dropped through 2" on the center of the crystal. The vertical scale is .005 volts per div. while the horizontal scale is 10 μs. per division. A 25 megacycle X-cut quartz crystal was used in obtaining these curves. The pickup was originally constructed for purposes of measuring the impact of the jet on the boundary. For this purpose it was a complete failure, because even the 1/16" diameter center area was much larger than the jet, and also because of poor high frequency response. It did,

however, provide a means of measuring the pressure of the gases in the cavity, because the minimum base diameter of the cavities were larger than 1/16", and the frequencies involved were not as high.

Experimental measurements of pressures resulting from a compression of gases in the cavity at different spark gap distances from the solid boundary are shown in figure 15. The spark energy was kept constant

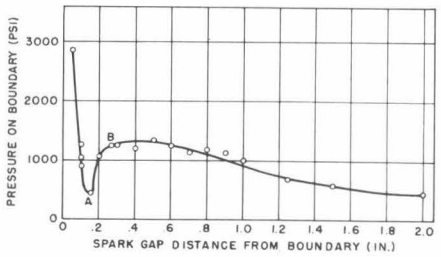

Figure 15. Pressures on the solid boundary arising from a compression of gases in the cavity.

during these observations and spherical cavities which were produced had a maximum radius of approximately .16". Figure 16 shows a picture of the cavity corresponding to point A of figure 15 at maximum R_o, and a few frames at the time of the compression pulse. Figure 17 shows the same frames for the cavity corresponding to point B in figure 15.

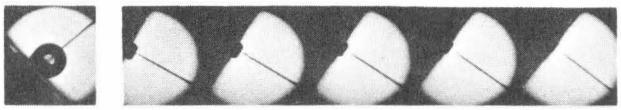

Figure 16. The cavity corresponding to point A in figure 15.

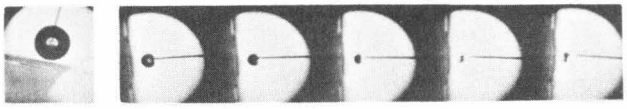

Figure 17. The cavity corresponding to point B in figure 15.

It is seen that pressures on the boundary resulting from a compression of gases inside the cavity for cavities in contact with the boundary

decrease rapidly as the perturbation of the hemispherical shape is increased. This is probably because the collapse process becomes less spherically symmetric. The pressure starts rising again when the distance of the spark gap from the boundary becomes large enough so that the cavities collapse away from the boundary, and the collapse becomes more spherically symmetric. A maximum is reached when the gain in pressure due to more spherically symmetric collapse is cancelled by the inverse square dropoff with increasing distance from the boundary and afterwards pressures on the boundary diminish gradually. It is of interest to note that shock wave pressures on the boundary can be higher than pressures resulting from a compression of gases of cavities which collapse on the boundary. These shock wave pressures are, however, quite low for the spark bubbles which were considered here, and although such pressures could increase greatly if cavities contained less permanent gas, it seems unlikely that shock waves will play an important role in cavitation damage.

The only information regarding the impact of the jet on the solid boundary was obtained from a study of the damage by cavities of this nature on aluminum samples. Figure 18 shows a typical cavity used in the damage studies at $R_o/R_o(0)$ values of approximately 1, .8, .6 and .46, and close to minimum volume. The pit produced by this cavity in an anealed and chemically polished high purity aluminum sample is shown in figure 19. The scale in figure 18 is 0.004" per division, and the minimum base diameter of the cavity in figure 19 is 0.179". The pit diameter is thus only 1/15 of the minimum cavity base diameter, so that the possibility that the pit could have been caused by a compression of the gases in the cavity can be ruled out, and the impact of the jet must have been

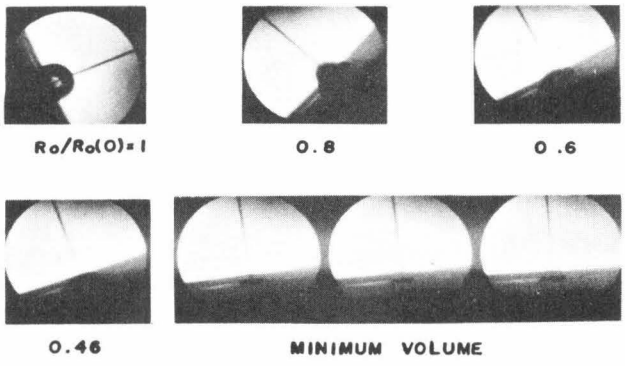

Figure 18. A cavity used in the damage studies.

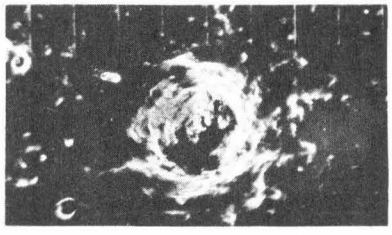

Figure 19. The pit produced in high purity aluminum by the cavity in figure 18.

responsible.

Damage studies of this nature yielded some information that cannot easily be explained in terms of the predicted mechanism. Cavities with somewhat larger initial perturbations of the hemispherical shape than the one shown in figure 18 failed to cause visible damage of the soft aluminum samples. For these cavities the estimated impact velocities of the jet were higher than the 300 ft/sec which was estimated for the cavity in figure 18. Another parameter thus appears to be playing a role as far as the damage is concerned. It was speculated that this parameter could be the radius of curvature of the tip of the jet.

A reduction of the initial perturbations of the hemispherical shape to values smaller than those of figure 18 drastically increased the damage potential of the cavities. A single cavity with $R_o(0) = .232''$, $R_2(0) = .012''$, $R_4(0) = .0114''$, $B_2 = -3.25$, $B_4 = 2.00$ and $T = 524\,\mu s$. could produce a pit in an aluminum alloy with a yield strength of 50,000 p.s.i. No experi-

mental explanation for this increase in the impact pressure could be found because the detailed behavior of the indented portions of the cavity wall could not be observed. The theory suggests a possible explanation which will be discussed briefly. The theoretical curves of $R_2/R_2(0)$ and $R_4/R_4(0)$ for this cavity are demonstrated in figures 20 and 21. The distance, D, of the tip of the jet from the solid boundary is shown in figure 22 as a function of $R_o/R_o(0)$. The dotted line in this figure corresponds to the cavity of figure 18.

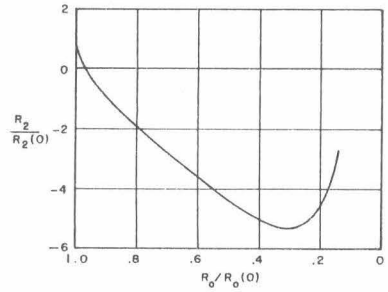

Figure 20. $R_2/R_2(0)$ as a function of $R_o/R_o(0)$ for the second cavity discussed under the damage studies.

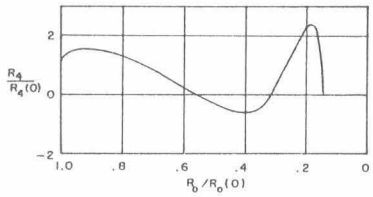

Figure 21. $R_4/R_4(0)$ as a function of $R_o/R_o(0)$ for the second cavity discussed under the damage studies.

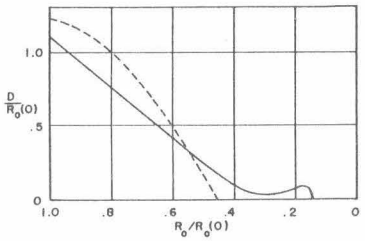

Figure 22. The reduced distance $D/R_o(0)$ of the tip of the jet from the solid boundary for the two cavities discussed under the damage studies.

It is thus seen that in the present situation, the jet which enters the cavity performs one complete oscillation before it strikes the boundary, while the jet entering the cavity in figure 18 continues its motion toward the boundary until the impact occurs. This oscillatory behavior could be the reason for the increased damage potential that was observed, because the impact velocity is greatly increased. The theoretical impact velocity in this case is 3350 ft/sec as compared to a mere 300 ft/sec for the cavity in figure 18.

CONCLUSIONS

1. Experimental results on the shape of cavities collapsing in contact with a boundary confirmed the theory derived by means of the second perturbation procedure.

2. Jets which enter cavities and damage the solid boundary through direct impact were observed experimentally. The occurrence of these jets is in agreement with suggestions of the theory.

3. The theory provided a partial explanation of the increase in damage potential of cavities when initial perturbations of the hemispherical shape were reduced. In addition to the impact velocity of the jet, another parameter, possibly the radius of the tip of the jet, seemed to influence the damage.

4. Shock wave pressures due to cavities of 0.16" radius collapsing away from the solid boundary under 1 atmosphere pressure difference were measured. These pressures had a maximum of about 1300 psi, and even though spark bubbles may contain more permanent gas than actual cavitation bubbles, it appears unlikely that cavities collapsing away from a boundary play an important role in cavitation damage.

BIBLIOGRAPHY

1. Plesset, M.S. and Mitchell, T.P., "On the Stability of the Spherical Shape of a Vapor Cavity in a Liquid", Quarterly of Applied Mathematics, Vol. 13, 1956, pp. 419-430.

2. Eisenberg, P., "On the Mechanism and Prevention of Cavitation", David Taylor Model Basin, Report 712 (1950) pp. 51-52.

3. Kornfeld, M., and Suvorov, L., "On the Destructive Action of Cavitation", J. of Applied Physics, Vol. 15, No. 6, 1944, pp. 495-496.

4. Erdelyi et al, Higher Transcendental Functions, Vol. 1, McGraw-Hill, 1958, pp. 56, 105-106.

5. Wayland, H., Differential Equations in Science and Engineering, Van Nostrand, 1957, p. 120.

6. Gilmore, F.R., "The Growth or Collapse of a Spherical Bubble in a Viscous Compressible Liquid", California Institute of Technology, Hydrodynamics Laboratory Report 26-4, 1952.

7. Schlichting, H., "Boundary Layer Theory, McGraw-Hill, 1955, pp. 64-65.

8. Cole, R.H., Underwater Explosions, Princeton University Press, 1948, pp. 338-341.

9. Ellis, A.T., "Observations on Cavitation Bubble Collapse", California Institute of Technology, Hydrodynamics Laboratory Report 21-12, 1952.

DISTRIBUTION LIST

6	Chief, Bureau of Naval Weapons, Wash. 25, D.C.	Code DLl-3	(1)
		RAAD-3	(1)
		RRRE	(1)
		RRRE-7	(1)
		RUAW-4	(2)
5	Chief, Bureau of Ships, Wash. 25, D.C.	Code 335	(1)
		421	(2)
		442	(1)
		644	(1)
3	Chief of Naval Research, Wash. 25, D.C.	Code 429	(1)
		438	(1)
		466	(1)
4	David Taylor Model Basin, Wash. 7, D.C.	Code 142	(1)
		500	(1)
		526	(1)
		591	(1)
1	Chief, Bureau of Yards and Docks, Wash. 25, D.C. (Research Div.)		
1	Naval Engineering Experiment Station, Annapolis, Md. (Librarian)		
1	Naval Academy, Annapolis, Md. (Librarian)		
1	Naval Postgraduate School, Monterey, Calif. (Librarian)		
1	Naval Weapons Laboratory, Dahlgren, Va. (Librarian)		
1	Naval Underwater Ordnance Station, Newport, R.I. (Librarian)		
2	Naval Ordnance Laboratory, Silver Springs, Md.		
		Desk HL (Library)	(1)
		Desk XL (Aeroballistics)	(1)
1	Naval Civil Engineering Laboratory, Port Hueneme, Calif. (Librarian)		
7	Naval Ordnance Test Station, Pasadena, Calif.	Code P508	(2)
		P804	(2)
		P8074	(1)
		P8076	(1)
		P80962	(1)
1	Naval Research Laboratory, Wash. 25, D.C. (Librarian)		
1	Navy Underwater Sound Laboratory, New London, Conn. (Librarian)		
1	Navy Electronics Laboratory, San Diego, Calif. (Librarian)		
1	Naval Air Development Center, Johnsville, Pa. (Librarian)		
1	Navy Mine Defense Laboratory, Panama City, Fla. (Librarian)		
1	Naval Ordnance Test Station, China Lake, Calif. (Code 7533)		
4	British Joint Services Mission (Naval Staff) via BuWeps DSC-3		
1	Defense Research Member (W), Canadian Joint Staff, via BuWeps DSC-3		
1	ASTIA Reference Center, Library of Congress, Wash. 25, D.C.		
6	Document Service Center, ASTIA, Arlington, Va.		
1	Office of Technical Services, Dept. of Commerce, Wash., D.C.		
6	National Aeronautics and Space Administration, Wash., D.C.		
1	National Bureau of Standards (Fluid Mechanics Div.) Wash., D.C.		
1	Coordinator for Research, Maritime Administration, Wash., D.C.		
1	National Science Foundation (Engr. Sciences Div.), Wash., D.C.		
1	Air research and Development Command, Wash., D.C.		
1	Air Force Office of Scientific Research (Mechanics Div.), Wash, D.C.		
1	Office of Ordnance Research, Durham, N.C.		
1	Committee on Undersea Warfare, NAS-NRC, Wash., D.C.		

1 Waterways Experiment Station, Vicksburg, Miss.
1 Merchant Marine Academy, Kings Point, L.I., N.Y. (Librarian)
2 Massachusetts Institute of Technology, Cambridge, Mass.
Dept. of N.A. and M.E., Prof. L. Troost (1)
Hydrodynamics Lab., Prof. A. Ippen (1)
1 Applied Physics Laboratory, Univ. of Washington, Seattle, Wash. (Librarian)
1 St. Anthony Falls Hydraulic Lab., Univ. of Washington, Seattle, Wash., (Librarian)
2 Stanford University, Stanford, Calif.
Dept. of Mech. Engr., Prof. B. Perry (1)
Head, Dept. of Math. (1)
1 Cornell University, Ithaca, N.Y. (Director, Grad. Sch. of Aero. Engr.)
2 Harvard University, Cambridge 38, Mass.
Dept. of Engr. Sci., Prof. G.F. Carrier (1)
Dept. of Math., Prof. G. Birkhoff (1)
1 University of Wisconsin Mathematical Research Center, Madison, Wisc. (Prof. L.M. Milne-Thomson)
1 Alden Hydraulic Laboratory, Worcester Polytechnic Institute, Worcester, Mass.
1 Garfield Thomas Water Tunnel, Ordnance Res. Lab., Penna. State University, University Park, Pa.
1 Davidson Laboratory, Stevens Institute of Technology, Hoboken, N.J.
1 The John Hopkins University, Baltimore, Md. (Dept. of Mech. Engr., Prof. S. Corrsin)
1 Colorado State University, Fort Collins, Colo. (Dept. of Civil Engr., Prof. M. Albertson)
2 University of Michigan, Ann Arbor, Mich.
Dept. of N.A. and M.E., Prof. R.B. Couch (1)
Dept. of Civil Engr., Prof. V. Streeter (1)
1 Polytechnic Institute of Brooklyn, Brooklyn, N.Y. (Head, Dept. of Aero. Engr. and Appl. Mech.)
2 Brown University, Providence, R.I., Div. of Appl. Math. (1)
Div. of Engr. (1)
2 Univ. of California, Berkeley, Calif., College of Engr.
Prof. A. Shade (1)
Prof. J.V. Wehausen (1)
1 Webb Institute of Naval Architecture, Glen Cove, L.I., N.Y. (Librarian)
1 New York State Maritime College, Fort Schuyler, N.Y. (Librarian)
1 University of Kansas, Lawrence, Kan. (Dean J.S. McNown)
1 Lehigh University, Bethlehem, Penna. (Dept. of Civil Engr., Prof. J.B. Herbich)
1 University of Notre Dame, Notre Dame, Indiana (Dept. of Engr. Mech., Prof. A.G. Strandhagen)
1 Rensselear Polytechnic Institute, Troy, N.Y. (Depth of Math., Prof. H. Cohen)
31 California Institute of Technology, Pasadena, Calif.
Prof. F. C. Lindvall (1)
Prof. D. Rannie (1)
Prof. C. B. Millikan (1)
Prof. M. S. Plesset (1)
Prof. T. Y. Wu (1)
Prof. V. A. Vanoni (1)
Hydrodynamics Lab. (25)

1 University of Illinois, Urbana, Ill. (Coll. of Engr., Prof. J. Robertson)
1 Scripps Institution of Oceanography, University of California, La Jolla, Calif. (Librarian)
1 Woods Hole Oceanographic Institution, Woods Hole, Mass. (Librarian)
1 Case Institute of Technology, Cleveland, Ohio (Librarian)
1 Institute of Fluid Mechanics and Applied Mathematics, University of Maryland, College Park, Md. (Librarian)
1 Philco Corporation, Philadelphia, Penna. (Engr. Librarian)
1 Vitro Corporation, Silver Springs, Md. (Engr. Librarian)
1 Gibbs and Cox, New York, N. Y. (Dr. S. Hoerner)
1 Eastern Research Group, Brooklyn, N. Y. (Dr. L. Meyerhoff)
1 Hydronautics, Rockville, Md. (Mr. P. Eisenberg)
1 Technical Research Group, New York, N. Y. (Dr. P. Kaplan)
1 Aerojet General Corporation, Azusa, Calif. (Mr. J. Levy)
1 The Martin Company, Baltimore, Md. (Science Technical Librarian)
1 Lockheed Aircraft Corporation, Burbank, Calif. (Engr. Librarian)
1 Douglas Aircraft Company, El Segundo, Calif. (Mr. A. M. O. Smith)
1 Bell Aerosystems Company, Buffalo, N. Y. (Engr. Librarian)
1 McDonnel Aircraft Company, St. Louis, Mo. (Engr. Librarian)
1 Chance Vought Aircraft, Inc., Dallas, Texas (Engr. Librarian)
1 Republic Aviation Corporation, Farmingdale, L. I., N. Y. (Engr. Librarian)
1 EDO Corporation, College Point, N. Y. (Engr. Librarian)
1 The RAND Corporation, Santa Monica, Calif. (Librarian)
1 Electric Boat Division, General Dynamics Corporation, Groton, Conn. (Engr. Librarian)
1 Hydrodynamics Laboratory, Convair Division, General Dynamics Corp., San Diego, Calif.
1 Goodyear Aircraft Corporation, Akron, Ohio (Engr. Librarian)
1 Grumman Aircraft Engineering Corporation, Bethpage, L. I., N. Y. (Engr. Librarian)
1 Aeronutronic Division, Ford Motor Company, Newport Beach, Calif. (Engr. Librarian)
1 Southwest Research Institute, San Antonio, Texas (Dept. of Appl. Mech.)
1 Boeing Airplane Company, Seattle, Wash. (Aero-Space Librarian)
1 Hughes Tool Company, Culver City, Calif. (Librarian)
1 United Technology Corporation, Sunnyvale, Calif. (Dr. D. A. Rains)
2 Cleveland Pneumatic Industries, Inc., Advanced Systems Development Div., El Segundo, Calif. Mr. S. Thurston (1)
Mr. W. Ellsworth (1)
1 Westinghouse Electric Corporation, Baltimore Division, Friendship Int'l Airport, Md. (Engr. Librarian)
1 General Electric Corporation, Ordnance Dept., Pittsfield, Mass. (Engr. Librarian)
1 General Electric Corporation, LME Dept., Schenectady, N. Y. (Engr. Librarian)
1 Clevite Brush Development, Clevite Research Center, Cleveland, Ohio (Engr. Librarian)
1 AVCO Manufacturing Company, Everett, Mass. (Engr. Librarian)
1 Society of Naval Architects and Marine Engineers, New York, N. Y.
1 Applied Mechanics Reviews, New York, N. Y.
1 Engineering Societies Library, New York, N. Y.
1 Institute of the Aerospace Sciences Library, New York, N. Y.